Landsat Time Series and Lidar as Predictors of Live and Dead Basal Area Across Five Bark Beetle-Affected Forests

Benjamin C. Bright, Andrew T. Hudak, Robert E. Kennedy, and Arjan J. H. Meddens

Abstract—Bark beetle-caused tree mortality affects important forest ecosystem processes. Remote sensing methodologies that quantify live and dead basal area (BA) in bark beetle-affected forests can provide valuable information to forest managers and researchers. We compared the utility of light detection and ranging (lidar) and the Landsat-based detection of trends in disturbance and recovery (LandTrendr) algorithm to predict total, live, dead, and percent dead BA in five bark beetle-affected forests in Alaska, Arizona, Colorado, Idaho, and Oregon, USA. The BA response variables were predicted from lidar and LandTrendr predictor variables using the random forest (RF) algorithm. RF models explained 28%–61% of the variation in BA responses. Lidar variables were better predictors of total and live BA, whereas LandTrendr variables were better predictors of dead and percent dead BA. RF models predicting percent dead BA were applied to lidar and LandTrendr grids to produce maps, which were then compared to a gridded dataset of tree mortality area derived from aerial detection survey (ADS) data. Spearman correlations of beetle-caused tree mortality metrics between lidar, LandTrendr, and ADS were low to moderate; low correlations may be due to plot sampling characteristics, RF model error, ADS data subjectivity, and confusion caused by the detection of other types of forest disturbance by LandTrendr. Provided these sources of error are not too large, our results show that lidar and LandTrendr can be used to predict and map live and dead BA in bark beetle-affected forests with moderate levels of accuracy.

Index Terms—Forestry, image sequence analysis, remote sensing, vegetation mapping.

I. INTRODUCTION

BARK beetle-caused tree mortality is prevalent across western North America [1] and affects forest primary productivity [2]–[4], carbon and nutrient cycling [5]–[8], forest

B. C. Bright and A. T. Hudak are with the Rocky Mountain Research Station, U.S. Forest Service, Moscow, ID 83843 USA (e-mail: benjamincbright@fs.fed.us; ahudak@fs.fed.us).

R. E. Kennedy is with the Department of Earth and Environment, Boston University, Boston, MA 02215 USA (e-mail: kennedyr@bu.edu).

A. J. H. Meddens is with the Department of Geography, University of Idaho, Moscow, ID 83844 USA (e-mail: ameddens@uidaho.edu).

Color versions of one or more of the figures in this paper are available online at http://ieeexplore.ieee.org.

hydrology [9]–[11], forest-atmosphere exchanges of water and energy [12]–[15], habitat selection by wildlife [16], [17], and wildfires [18], [19]. With synoptic measurements, remote sensing technologies may help forest managers understand and manage tree mortality from bark beetles, but such information must be expressed in terms familiar to managers, such as stand basal area (BA), defined as the cross-sectional area of tree stems for a given area. Here, we compare how well two sources of remotely sensed data, light detection and ranging (lidar), and Landsat time-series data analyzed using the Landsat-based detection of trends in disturbance and recovery (LandTrendr) algorithm [20], can predict live and dead stand BA in bark beetle-affected forests.

Bark beetles have killed billions of trees across millions of hectares in western North America in the last two decades [1]. Adult bark beetles bore through the outer bark of tree stems and lay eggs in the phloem beneath the outer layer of the bark that carries carbohydrates from foliage to roots. Larvae hatch and feed on the phloem, excavating tunnels as they feed. Through mass attack coordinated by pheromones, large numbers of bark beetles are able to kill trees by girdling [21], [22]. Weaker trees such as those suppressed by other trees or affected by drought are more susceptible to being killed by bark beetles [23]–[25]. The availability of abundant host trees and elevated temperatures (particularly higher winter minimum temperatures) has facilitated bark beetle population increase and range expansion [23], [24], [26].

Studies have shown that remote sensing can detect and map insect-caused tree damage and mortality across large spatial extents [27]–[30]. Dead trees reflect incoming radiation differently than live trees, making the detection of tree mortality by passive remote sensing systems possible [28], [31]–[33]. Changes in forest structure following tree mortality also make the detection of tree mortality by active remote sensing systems such as lidar possible [34], [35]. However, the nature of bark beetle outbreaks creates challenges for detecting bark beetle-caused tree mortality with moderate-resolution remote sensing. First, outbreaks often occur gradually and last several years so that attributing spectral and structural differences to tree mortality, especially low levels of tree mortality, can be difficult [27]. Second, during outbreaks, bark beetles selectively kill larger and more susceptible trees (e.g., [36]), leaving younger and healthier trees, so that beetle-affected forests are usually a mix of live and dead trees, which both contribute to the spectral and structural "signatures" of beetle-affected forests [27].

Lidar systems measure the time required for laser pulses to reflect off illuminated surfaces and return to the sensor; round-trip times of laser pulses are then converted to range or distance measurements. When lidar is flown over forests, information about tree canopy height and density can be created and forest attributes such as BA and biomass can be predicted with high accuracy [37]–[40]. Lidar has been shown to predict tree BA (and related attributes such as biomass) more accurately than single-date multispectral imagery [39], [40] due to the greater sensitivity of lidar to forest structure variability. Successful prediction of live and dead BA in bark beetle-affected forest using lidar alone has been demonstrated [35].

Landsat has proved to be an invaluable resource for describing and studying vegetation dynamics [41]. Landsat has some advantages over lidar that makes use of Landsat data for predicting forest stand BA responses appealing. Lidar data are expensive to acquire and process; contain only limited reflectance information; are limited both spatially and temporally; and have only recently become more widely available. Landsat data, on the other hand, are freely available; capture reflectance information in several spectral bands that provide information about vegetation properties; are acquired globally every 16 days at moderate spatial resolution; and the Landsat archive extends back to 1972, making image time-series detection of disturbance possible [41]. Recent methodologies such as the Vegetation Change Tracker [42], [43] and LandTrendr that make use of Landsat Thematic Mapper image archive (beginning in 1984) have shown promise for detecting forest disturbance and predicting stand BA [20], [44]–[46]. LandTrendr algorithms seek to simplify the temporal trajectory of a spectral index over the course of 16-day observations into a series of straight-line segments, generalized to an annual time step by default. The starting year, duration, and change in these segments can be used to describe the change process of interest on a per-pixel basis. Because the LandTrendr algorithms measure the evolution of processes on the landscape, they may capture the impact of the mortality process better than single-date measurements from other sensors. Meigs *et al.* [44], in a descriptive rather than predictive study, found that bark beetle-killed BA was related to LandTrendr trajectories. Pflugmacher *et al.* [45] predicted live and dead BA following a combination of wildfire (predominantly), harvest, and bark beetle disturbances and found that LandTrendr predicted dead BA more accurately than lidar.

Because multispectral data primarily provide information about optical forest properties whereas lidar data primarily provide information about vertical forest structure, researchers have investigated using both types of remotely sensed data to estimate forest variables of interest. Forest variables predicted using both multispectral and lidar data include: BA [39], tree density [39], [47], tree volume [40], [47]–[50], aboveground tree biomass [40], [50], and fuels [51], [52]. Using both types of data usually results in better prediction accuracies than if only one type of data is used.

In the United States, bark beetle-caused tree mortality is mapped annually via aerial detection surveys (ADSs) [53]. Observers estimate the location, affected area, and severity of bark beetle disturbance from aircraft. Mortality information is delivered in the form of georeferenced digital polygon data. Although useful for resource management and scientific applications, ADS data have some limitations that cause uncertainty in tree mortality estimates: not all forests are surveyed every year; the skill and experience of observers vary; and affected area, rather than mortality area, is reported. To overcome the latter limitation, Meddens *et al.* [1] derived a 1-km gridded dataset of tree mortality area from ADS affected-area polygon data.

Random forest (RF) modeling has been shown to be an effective tool for predicting forest attributes from remotely sensed explanatory variables [40], [54]–[56]. The RF algorithm creates a large number of classification trees. Observations are classified by each tree and are assigned to the majority class. Variable importance scores are generated by ranking variables according to how often they decrease the mean-squared error. Some advantages of RF modeling include the ability to predict continuous, non-normal variables; generation of variable importance scores; and the random withholding of data during bootstrap iterations that makes the division of data into training and evaluation datasets unnecessary for most applications.

Here, we evaluate the utility of lidar and LandTrendr to predict field-observed total, live, dead and percent dead stand BA. Our objectives were 1) to compare performance of predictive RF models of these responses that use LandTrendr, lidar, or both as predictors, and 2) to further evaluate models by comparing predicted percent dead stand BA to estimates of tree mortality area generated from the gridded ADS dataset of Meddens *et al.* [1], a similar independent dataset. We evaluated models predicting both dead and percent dead stand BA because 1) both were important variables that were not necessarily correlated, and 2) we considered percent dead stand BA to be approximately equivalent to ADS mortality estimates of Meddens *et al.* [1]. As demonstrated by others, we expected lidar to be more sensitive than multispectral imagery to overall stand structure [39], [40], and LandTrendr to be more sensitive than lidar to stand health conditions and disturbance history [45]. Therefore, we hypothesized that lidar would predict total and live stand BA more accurately, whereas LandTrendr would predict dead and percent dead stand BA more accurately.

II. METHODS

A. Study Areas

Study areas included five coniferous forests across western North America that have been affected by bark beetles: Kenai Peninsula in Alaska (AK), Pinaleño Mountains in Arizona (AZ), north central Colorado (CO), central Idaho (ID), and central Oregon (OR) (Fig. 1). Spruce beetles (*Dendroctonus rufipennis* Kirby) have affected forests in AK and AZ, whereas mountain pine beetles (*Dendroctonus ponderosae* Hopkins) have affected forests in CO, ID, and OR. Coincident field observations, LandTrendr outputs, and lidar data were available for each study area. LandTrendr output extents encompassed and extended beyond lidar acquisition extents (Fig. 1).
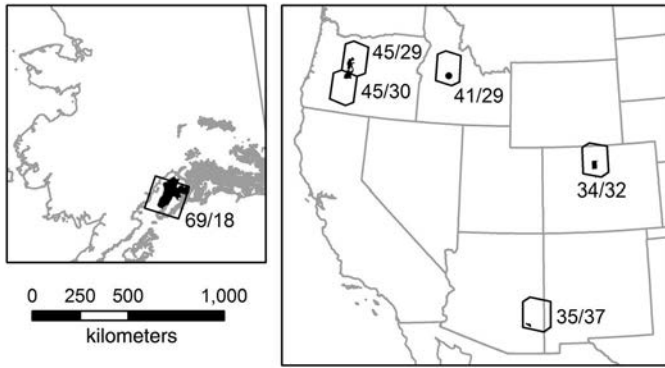
Fig. 1. Study areas in Alaska, Arizona, Colorado, Idaho, and Oregon, USA. Lidar extents are shown as filled black polygons (except in Idaho where it is shown as a black dot). LandTrendr data extents are shown as hollow polygons. Landsat Path/Row numbers are given next to each LandTrendr data extent.

B. Field Observations

Tree diameter at breast height (DBH) and health (live or dead) were measured for each tree in circular fixed-radius plots within lidar extents of all study areas. Plots were geolocated via GPS so that comparison with lidar and LandTrendr data was possible. Plot design varied between study areas. In AK and OR, USFS Forest Inventory and Analysis (FIA) plots were systematically located. In AZ, 80% of the plots were systematically located within the extent of the lidar survey and 20% of the plots were supplementary plots added at random locations at higher altitude in the spruce-fir zone with higher tree mortality, which the systematic plots failed to sample. In CO and ID, plots were located according to stratified random sampling designs. Radii of AZ, CO, and ID plots were 12.6, 8.0, and 11.3 m, respectively. FIA plots in AK and OR consisted of four subplots with 7.3 m radii. In OR, USFS Region 6 Continuous Vegetation Survey (CVS) plots were also included; CVS plots consist of five subplots with 15.5 m radii. Most plot observations were gathered in 2010, although some FIA plot observations were gathered as early as 2004. Distributions of %Dead BA as measured at plots differed between study areas (Fig. 2). Tree measurements of FIA and CVS subplots were combined, and tree measurements were summarized by live and dead stand BA, in units of $m^2 ha^{-1}$, for each plot using the Forest Vegetation Simulator (FVS) [57], [58].

C. Lidar

Discrete-return lidar data were acquired over each study area between the years 2008 and 2010 (Table I). For each study area, returns were classified as vegetation or ground by the vendor; ground return elevations were averaged for each 1-m grid cell to produce a bare-earth digital terrain model (DTM) of 1-m resolution; and DTM values were subtracted from vegetation returns to calculate height-above-ground values of vegetation returns. All vegetation returns (as opposed to only first returns) within each plot extent were then summarized to produce lidar metric variables to be used as predictor variables in models (Table II). Rather than producing lidar metrics for each FIA and CVS subplot, vegetation returns of FIA and CVS subplots

were combined by plot before producing plot-level lidar metrics. Lidar metric grids of 30-m spatial resolution (comparable to LandTrendr output resolution) were also produced for mapping purposes. Lidar data processing was done using FUSION software [59].

D. LandTrendr

For each study area, Landsat Thematic Mapper (TM) time-series images from 1984 to 2010 were processed through LandTrendr acting on individual pixels and operating on an annual time step [20]. The normalized difference ratio of Landsat bands 4 and 7 $((\mathrm{band}4 - \mathrm{band}7)/(\mathrm{band}4 + \mathrm{band}7))$ [60] was used for temporal segmentation, and disturbance was defined as any segment showing a decline in this index (Fig. 3). Once disturbance segments were defined, their timing was imposed on the three tasseled-cap (TC) bands of brightness (TCB), greenness (TCG), and wetness (TCW) [61] and pre- and post-disturbance values for TCB, TCG, and TCW and their differences (ΔTCB, ΔTCG, and ΔTCW) were calculated (Table III). Other metrics included the greatest disturbance (GD) and the longest disturbance (LD) for every pixel, in terms of when the disturbance started and the duration of the disturbance (Fig. 3; Table III). Values of these metrics coincident with plot extents were extracted from the LandTrendr outputs to be used as candidate predictor variables in RF models (Table III).

E. ADS Data

To evaluate lidar and LandTrendr model performance, predictions of %Dead BA were compared to a recently published gridded ADS dataset [1]. Meddens et al. [1] describe the process of converting ADS affected-area polygons (polygon extents include live trees) to tree mortality area (crown area of killed trees) grids covering the western United States. We briefly summarize the process here. ADS polygons reporting the number of bark beetle-killed trees for each year from 1997 to 2010 were converted to 1-km^2 grids. Grid cell values of the number of killed trees were converted to grid cell values of crown mortality area by multiplying the number of killed trees by their tree host crown area. Comparison of these grids with high-resolution imagery showed that ADS data underestimated mortality. To compensate for underestimation, adjustment factors (3.7–20.9 depending on tree species) were applied to grids to create an upper estimate of tree mortality area within each grid cell. Subsequent processing of the dataset in the western United States included the extension of the dataset to 2012 (previously from 1997 to 2010) and addition of a middle estimate [62]. The middle estimate was based on subsequent remote sensing analyses in other regional study areas and improved upon the upper estimate by reducing the adjustment factor for mountain pine beetle in lodgepole pine from 20.9 to 13.6. For this analysis, we summed mid-level tree mortality area grids from 1997 to 2010 to create a 1-km map of cumulative bark beetle-caused tree mortality area across the contiguous United States.

The dataset of Meddens et al. [1] does not include AK. To produce a similar 1-km ADS map of cumulative spruce
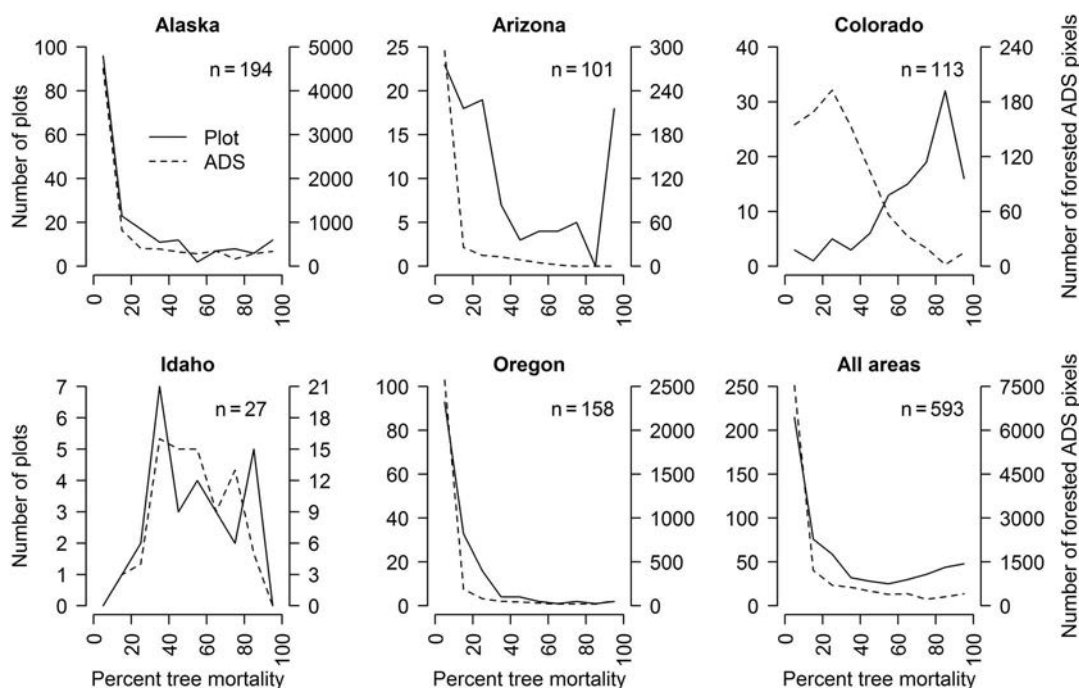
Fig. 2. Histograms showing percent tree mortality as measured on field plots and estimated by ADS data across forested lidar extents of the five study areas. The number of field plots in each study area is given in the upper right corner of each panel. Field plot histograms are in terms of percent dead BA. ADS histograms are in terms of percent tree mortality area.

TABLE I
LIDAR SURVEY PARAMETERS

Study area	Sensor	Acquisition date	Average pulse density (pulses m^{-2})	Maximum scan angle (°)	Flying height above ground (m)
Alaska	Optech ALTM Gemini	May–Sep. 2008	0.3	±16	1800
Arizona	Leica ALS50 Phase II	Sep. 22–27, 2008	7.4	±15	1200
Colorado	Optech 3100 AE	Aug. 2010	2	±18	1250
Idaho	Leica ALS50 Phase II	Aug. 4–5, 2010	8.7	±13	900
Oregon	Leica ALS50 Phase II	Oct. 2009–Sep. 2010	8.6	±14	900 and 1300

beetle-caused tree mortality area across the Kenai Peninsula, we followed the methods of Meddens *et al.* [1] using AK ADS polygon data from 1989 to 2010. For the Kenai Peninsula, ADS polygons before 1999 and 41% of polygons from 2000 to 2010 did not include the number of trees killed as an attribute. Rather than excluding these polygons, which represented a substantial amount of tree mortality, we assumed a tree mortality density of five trees per acre, the median reported tree mortality density of ADS polygons across the Kenai Peninsula for 1999–2010.

F. Random Forest

RF modeling, as implemented in the randomForest package of R (version 4.6–7) [54], [63], [64], was used to predict Total, Live, Dead, and %Dead BA response variables from lidar and LandTrendr predictor variables. Default settings were used for RF iterations: the number of variables tried at each split equaled the number of predictor variables divided by three; 500 trees were grown; and the minimum size of terminal nodes was five. We combined observations from all study areas, which had different numbers of plots (194, 101, 113, 27, and 158 plots for AK, AZ, CO, ID, and OR, respectively), to create RF models.

To equally represent each study area in RF models, we weighed each observation by the inverse number of plots for that study area, i.e., ID and AK observations were assigned weights of 0.037 (1/27) and 0.005 (1/194), respectively. Then, a weighted random sample of two-thirds of all observations was taken before each RF iteration, so that observations from study areas with fewer plots had a higher probability of being selected. As such, all RF model iterations were based on 395 of the total 593 observations.

For each of the four BA response variables, RF models that used only lidar, only LandTrendr, and combined lidar and LandTrendr response variables were produced, so that a total of 12 final models were created. For each of these 12 models, we repeated the RF variable selection methodology of Murphy *et al.* [65] 100 times to create model improvement ratio (MIR) [65]–[67] distributions for each predictor variable. The RF variable selection process of Murphy *et al.* [65], which we used because we wished to create parsimonious models that maximized percent variance explained, was as follows: an RF model that included all candidate predictor variables was created and MIR values, defined as variable importance (mean decrease accuracy) divided by the maximum model improvement score

TABLE II
NAMES AND DESCRIPTIONS OF LIDAR CANDIDATE VARIABLES

Variable name	Description
HMIN	Minimum canopy height
HMAX	Maximum canopy height
HMEAN	Mean canopy height
HMODE	Mode canopy height
HSD	Standard deviation of canopy height
HCV	Coefficient of variation of canopy height
HIQD	Interquartile distance of canopy height
HSKEW	Skewness of canopy height
HKURT	Kurtosis of canopy height
HP5	5th percentile of canopy height
HP10	10th percentile of canopy height
HP25	25th percentile of canopy height
HP50	50th percentile of canopy height
HP75	75th percentile of canopy height
HP90	90th percentile of canopy height
HP95	95th percentile of canopy height
CRR	Canopy relief ratio, (HMEAN – HMIN) / (HMAX – HMIN) [73]
DENSITY	Percentage of all returns >1.37 m in height
STRAT0	Proportion of all returns <0.15 m in height
STRAT1	Proportion of all returns ≥0.15 m and <1.37 m in height
STRAT2	Proportion of all returns ≥1.37 m and <5 m in height
STRAT3	Proportion of all returns ≥5 m and <10 m in height
STRAT4	Proportion of all returns ≥10 m and <20 m in height
STRAT5	Proportion of all returns ≥20 m and <30 m in height
STRAT6	Proportion of all returns ≥30 m in height

Only returns > 1.37 m in height were used to create canopy height variables.
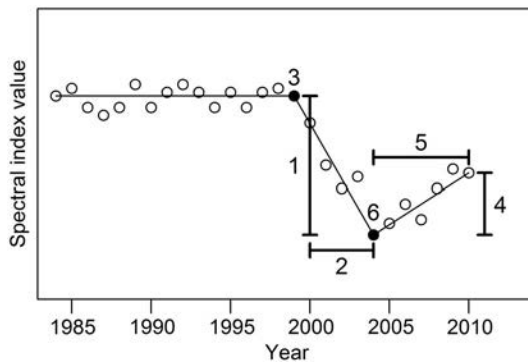

Fig. 3. Theoretical disturbed Landsat pixel trajectory depicting LandTrendr segments and variables. Hollow dots represent annual Landsat spectral index values. Lines represent segments temporally fitted by LandTrendr. Dimension lines represent LandTrendr variables: disturbance magnitude (1), duration (2), recovery magnitude (4), and recovery duration (5). Filled dots represent pre-disturbance (3) and post-disturbance (6) value variables. See Table III for LandTrendr variable names and descriptions.

so that MIR values range from zero (low importance) to one (high importance), were created for each predictor variable. Then, variables with MIR values below i, where $i = 0$, 0.1, 0.2, and so forth until 0.9, were dropped and an RF model was created. The RF model that minimized model MSE, maximized percent variance explained, and minimized the number of predictor variables was selected, and MIR values for selected predictor variables were returned. We repeated the process of Murphy *et al.* [65] 100 times because we found that for a given response variable, it often selected different RF models and

returned different MIR values for selected predictor variables, but through repetition, we could generate stable MIR distributions and means for predictor variables. Predictor variables with the highest mean MIR values, as determined by a threshold, were selected for final models. Mean MIR thresholds, which differed between the 12 models, were determined by finding mean MIR thresholds under which variables did not improve percent variance explained. If variables over mean MIR thresholds were correlated > 0.9, the variable with the lowest mean MIR value of the two was dropped, so that no final model contained variables correlated > 0.9.

G. Comparison With ADS Data

Final RF models predicting %Dead BA were applied to LandTrendr and lidar metric grids to create maps of %Dead BA for each study area. For comparison with the 1997–2010 cumulative tree mortality area map generated from ADS data [1], 30-m LandTrendr and lidar %Dead BA maps were aggregated to 1-km spatial resolution and Spearman correlations between predicted values of %Dead BA and % tree mortality area within 1-km^2 grid cells were calculated. Spearman correlations were used to account for the effect of non-normal distributions and a possible nonlinear relationship between %Dead BA and % tree mortality area. Only forested grid cells, which we determined using a forest mask developed from the forest type layer of Ruefenacht *et al.* [68], were included in Spearman correlation calculations. We also excluded grid cells where monitoring trends in burn severity (MTBS) data indicated that fire occurred between the years 1984 and 2010 [69].

TABLE III
NAMES AND DESCRIPTIONS OF LANDTRENDR CANDIDATE VARIABLES

Variable name	Description	Fig. 3 reference
GDmag	Magnitude of greatest disturbance	1
GDdur	Duration of greatest disturbance	2
GDpre.val	Cover value before greatest disturbance	3
GDpost.mag	"Recovery" magnitude after greatest disturbance	4
GDpost.dur	"Recovery" duration after greatest disturbance	5
GDpost.val	Cover value after greatest disturbance	6
GDpreTCB	Landsat tasseled cap brightness before greatest disturbance	3
GDpreTCG	Landsat tasseled cap greenness before greatest disturbance	3
GDpreTCW	Landsat tasseled cap wetness before greatest disturbance	3
GDΔTCB	Greatest change in Landsat tasseled cap brightness	1
GDΔTCG	Greatest change in Landsat tasseled cap greenness	1
GDΔTCW	Greatest change in Landsat tasseled cap wetness	1
GDpostTCB	Landsat tasseled cap brightness after greatest disturbance	6
GDpostTCG	Landsat tasseled cap greenness after greatest disturbance	6
GDpostTCW	Landsat tasseled cap wetness after greatest disturbance	6
GDΔpostTCB	"Recovery" of Landsat tasseled cap brightness after greatest disturbance	4
GDΔpostTCG	"Recovery" of Landsat tasseled cap greenness after greatest disturbance	4
GDΔpostTCW	"Recovery" of Landsat tasseled cap wetness after greatest disturbance	4
LDmag	Magnitude of longest disturbance	1
LDdur	Duration of longest disturbance	2
LDpre.val	Cover value before longest disturbance	3
LDpost.mag	"Recovery" magnitude after longest disturbance	4
LDpost.dur	"Recovery" duration after longest disturbance	5
LDpost.val	Cover value after longest disturbance	6
LDpreTCB	Landsat tasseled cap brightness before longest disturbance	3
LDpreTCG	Landsat tasseled cap greenness before longest disturbance	3
LDpreTCW	Landsat tasseled cap wetness before longest disturbance	3
LDΔTCB	Longest change in Landsat tasseled cap brightness	1
LDΔTCG	Longest change in Landsat tasseled cap greenness	1
LDΔTCW	Longest change in Landsat tasseled cap wetness	1
LDpostTCB	Landsat tasseled cap brightness after longest disturbance	6
LDpostTCG	Landsat tasseled cap greenness after longest disturbance	6
LDpostTCW	Landsat tasseled cap wetness after longest disturbance	6
LDΔpostTCB	"Recovery" of Landsat tasseled cap brightness after longest disturbance	4
LDΔpostTCG	"Recovery" of Landsat tasseled cap greenness after longest disturbance	4
LDΔpostTCW	"Recovery" of Landsat tasseled cap wetness after longest disturbance	4

TABLE IV
PERCENT VARIANCE EXPLAINED BY RF MODELS PREDICTING TOTAL, LIVE, DEAD, AND PERCENT
DEAD STAND BA ($m^2 ha^{-1}$) FROM DIFFERENT SETS OF PREDICTOR VARIABLES

Predictor variables	Response variable			
	Total BA	Live BA	Dead BA	%Dead BA
Lidar	53	61	34	29
LandTrendr	46	28	51	48
Combined	61	61	54	51

See Fig. 3 for further variable explanation.

III. RESULTS

In AK, ID, and OR, distributions of %Dead BA as determined by field plots approximated ADS distributions of % tree mortality area across forested lidar extents (Fig. 2). In AK and OR, distributions were positively skewed and in ID, distributions were closest to normal. In AZ and CO, field plot distributions of %Dead BA were bimodal and negatively skewed, respectively, whereas ADS distributions of % tree mortality area were positively skewed. Distributions of both %Dead BA and % tree mortality area aggregated across all study areas were positively skewed.

RF models explained 28%–61% of the variance in BA response variables (Table IV). Lidar models were better predictors of Total and Live BA, whereas LandTrendr models were better predictors of Dead and %Dead BA. RF models that combined both lidar and LandTrendr predictors performed slightly better than the models based on variables from a single sensor type.

Lidar density variables, especially DENSITY (Percentage of all returns > 1.37 m in height), as well as HMAX (Maximum canopy height), HMEAN (Mean canopy height), HP25 (25th percentile of canopy height), and CRR (Canopy relief ratio)

TABLE V
AVERAGE MODEL IMPROVEMENT RATIO (MIR) VALUES OF VARIABLES SELECTED AS IMPORTANT
FOR MODELS PREDICTING TOTAL, LIVE, DEAD, AND %DEAD BA FROM
LIDAR AND LANDTRENDR VARIABLES

Explanatory variable	Model improvement ratio			
	Total BA	Live BA	Dead BA	%Dead BA
Lidar				
HMAX			0.7	0.9
HMEAN		0.2		0.4
HMODE				0.5
HSKEW			0.6	
HP25	0.3	0.2	0.6	
CRR	0.2		0.8	0.5
DENSITY	0.7	1.0	0.6	0.7
STRAT0		0.4	0.5	0.4
STRAT2				0.6
STRAT3	0.2	0.2		
STRAT4	1.0	0.5	0.9	
LandTrendr				
GDmag	0.3	1.0		0.8
GDpre.val	0.6	0.6	0.2	0.4
GDpost.mag	0.2		0.4	
GDpost.dur			0.2	
GDpost.val		0.4		
GDpreTCB	0.3		0.3	
GDpreTCG	0.9	0.6	0.6	
GDpreTCW	0.4	0.3		
GDΔTCB			0.2	
GDΔTCW	0.3		0.8	0.6
GDpostTCG		0.4		
GDΔpostTCW			0.2	0.7
LDmag			0.2	0.4
LDpre.val	0.3		0.3	0.8
LDpreTCG	0.9		0.9	0.4
Combined				
HMEAN		0.1		
HP25	0.3	0.1		
CRR	0.1		0.2	
DENSITY	0.6	1.0		0.3
STRAT0	0.2	0.3		
STRAT3	0.1	0.1		
STRAT4	1.0	0.5	0.2	
GDmag				0.6
GDpre.val	0.2		0.2	0.3
GDpost.mag			0.3	
GDpreTCG	0.3		0.5	
GDΔTCW	0.2		0.6	0.5
GDΔpostTCW			0.2	0.6
LDmag			0.3	0.4
LDpre.val			0.3	1.0
LDpreTCG	0.2		1.0	0.4

A MIR value of 1 indicates most important. Only MIR values of selected variables are shown.

were important predictors of BA response variables (Table V). LandTrendr variables that were frequently chosen as important predictors of BA variables included GDmag (magnitude of greatest disturbance), GDpre.val (Cover value before greatest disturbance), GDpost.mag ("Recovery" magnitude after greatest disturbance), LDmag (Magnitude of longest disturbance), LDpre.val (Cover value before longest disturbance), LDpreTCG (Landsat TCG before longest disturbance), and greatest disturbance pre-, delta-, and posttasseled cap variables. GDmag, predisturbance cover values, and predisturbance TCG were important predictors of all BA variables. LDmag and changes in TCW were important predictors of Dead and %Dead BA. For combined models, lidar variables were generally chosen as most important when predicting Total and Live BA,

Study area	Lidar extent			LandTrendr extent
	Lidar	LandTrendr	Combined	LandTrendr
Alaska				
LandTrendr	0.33			
ADS	0.35	0.62	0.57	0.52
Arizona				
LandTrendr	0.13			
ADS	0.49	0.31	0.44	0.42
Colorado				
LandTrendr	0.65			
ADS	0.42	0.56	0.54	0.49
Idaho				
LandTrendr	0.13			
ADS	0.46	0.32	0.40	0.36
Oregon				
LandTrendr	0.02			
ADS	−0.16	0.31	0.33	0.28

Lidar- and LandTrendr-derived estimates were aggregated to 1-km resolution for comparison with ADS-derived estimates.
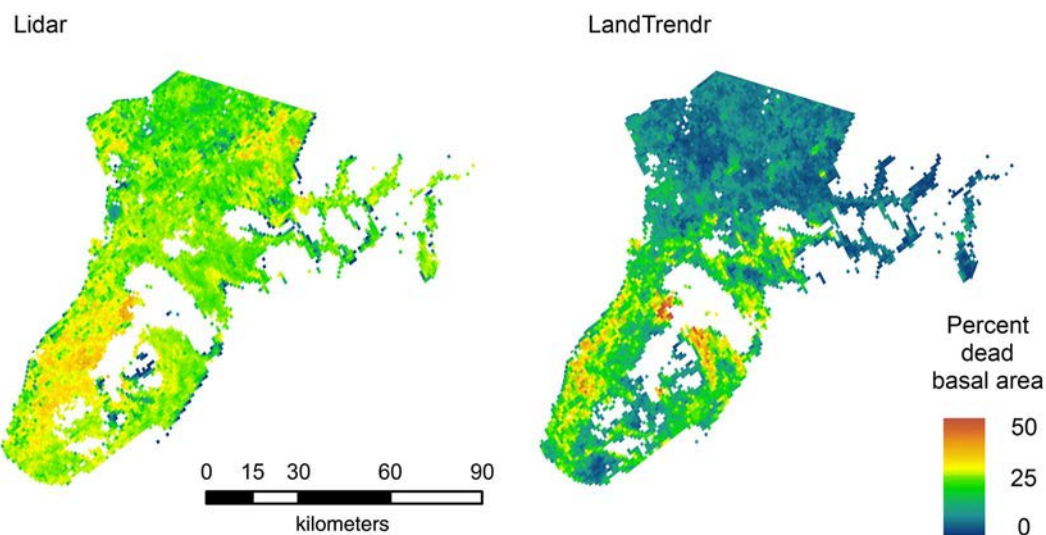

Fig. 4. Lidar- and LandTrendr-derived tree mortality maps of the Kenai Peninsula, Alaska. Nonforested and burned areas are masked in white. Map pixels are aggregated to 1-km spatial resolution.

whereas LandTrendr variables were generally chosen as most important when predicting Dead and %Dead BA.

Lidar- and LandTrendr-predicted %Dead BA were weakly to moderately correlated with ADS estimates of % tree mortality across unburned forested areas of lidar extents (Table VI; Fig. 4). Correlations between LandTrendr predictions and ADS estimates of % tree mortality were generally comparable to or greater than correlations between lidar predictions and the ADS estimates. LandTrendr predictions and ADS estimates of % tree mortality were weakly to moderately correlated across unburned forested areas of LandTrendr extents (r = 0.28 − 0.52; Table VI). Correlations between LandTrendr and ADS estimates were greatest in AK and CO (r = 0.49 − 62). Visual

comparison of maps showed that areas of greater %Dead BA in LandTrendr maps generally corresponded to areas of greater tree mortality area in the ADS map (Fig. 5).

In unburned forested areas, lidar-derived predictions of %Dead BA aggregated to 1-km^2 grid cells, averaged between 18% and 34%, and ranged from 0%–54% (Fig. 6). Across unburned forested lidar extents, LandTrendr-derived maps showed more variability in %Dead BA between study areas than lidar-derived maps, with predictions, aggregated to 1-km^2 grid cells, averaging 12%–43%, and ranging from 0%–69%. Average ADS estimates of % tree mortality area within unburned forested areas of lidar extents were generally lower (4%–29%), with greater variability (ranges between 0% and
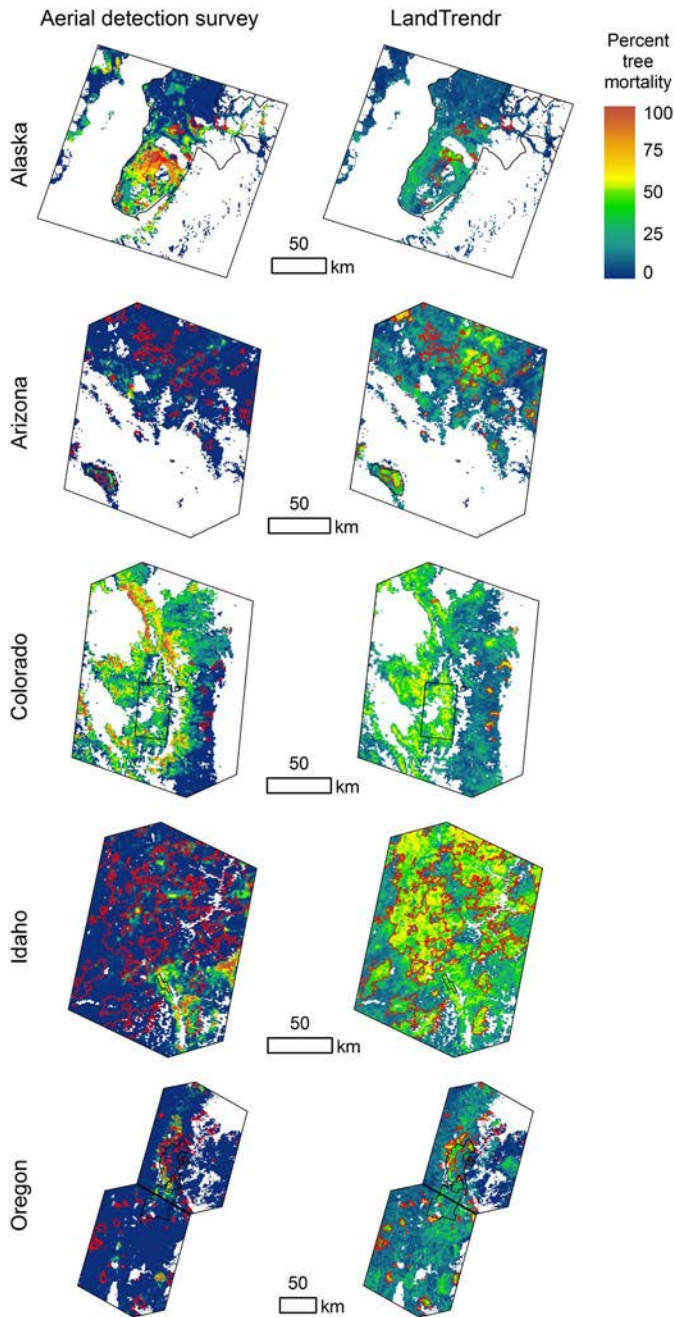
Fig. 5. ADS-derived and LandTrendr-derived tree mortality maps at 1-km resolution. Lidar extents, where plots are located, are outlined in black. Areas where monitoring trends in burn severity data indicate fire occurrence from 1984 to 2010 are outlined in red. Nonforested areas are masked in white. LandTrendr maps, which are in terms of percent dead BA, are aggregated to 1-km spatial resolution for comparison with ADS maps, which are in terms of percent tree mortality area.

100%), except in ID, where average ADS mortality was much greater (52%). In unburned forested areas within LandTrendr extents, LandTrendr predictions of %Dead BA aggregated to 1-km² grid cells, averaged between 11% and 25%, and ranged from 0% to 74%, whereas ADS estimates of % tree mortality area averaged between 2% and 29% and ranged from 0% to 100%.

IV. DISCUSSION

The RF algorithm was useful to our analysis for several reasons. First, distributional shapes of % tree mortality varied between study areas (Fig. 2). The RF predictive modeling approach is nonparametric and, therefore, well suited for these varying distributional shapes. RF allowed us to predict these variables without having to transform and back transform, which would have been necessary if parametric modeling was used. The distribution of %Dead BA of records from all study areas matched the distribution of % tree mortality area from ADS data, suggesting that plots sampled variability in tree mortality well. Second, variable importance values generated by RF let us identify the most important out of many candidate predictor variables so we could create and interpret parsimonious models. Third, processing time was not excessive despite running thousands of RF model iterations.

LandTrendr variables chosen as most important were logically related to BA variables. Total and Live BA were positively correlated to predisturbance cover and TCG, a measure of forest "greenness" related to canopy cover, leaf area index, and biomass [70]. Dead and %Dead BA were positively correlated with disturbance magnitude variables and greater changes in TCW; forest wetness has been shown to decrease following bark beetle-caused tree mortality [71]. Live BA was negatively correlated to disturbance magnitude. We also found predisturbance cover and predisturbance TCG to be positively correlated to Dead and %Dead BA, which agrees with the fact that bark beetle-caused tree mortality is often more severe in stands of greater BA [25], [72].

Maps of % tree mortality generated from lidar, LandTrendr, and ADS generally agreed with each other although large differences between maps did exist. Visual patterns of mortality severity were similar between maps, i.e., where the ADS map showed higher levels of tree mortality, lidar and LandTrendr maps usually showed higher levels of tree mortality. But lidar, LandTrendr, and ADS estimates of %tree mortality were moderately to poorly correlated. Correlations were not greater because each type of estimate was subject to error. Lidar and LandTrendr predictions were produced using RF models that explained only 29% and 48% of the variation in %Dead BA, respectively; thus, LandTrendr predictions were likely more accurate than lidar predictions, as greater correlation with the ADS data also suggests. However, estimates of tree mortality area from the ADS data contain a degree of uncertainty because of how different surveyors acquire data under different viewing conditions at different times with varying mortality severities. In addition, some forests might not have been entirely surveyed every year. Correlations between LandTrendr and ADS estimates across LandTrendr extents were low because LandTrendr detected all types of forest disturbance, whereas the ADS data only included bark beetle-caused tree mortality. We partly controlled confusion with other types of forest disturbance by excluding areas that burned from 1984 to 2010, as indicated by MTBS data, from our analysis. Wildfires were particularly numerous in ID and moderately numerous in AZ and OR. In AK and CO, bark beetle-caused tree mortality seemed to be the predominant type of forest disturbance, so that correlations
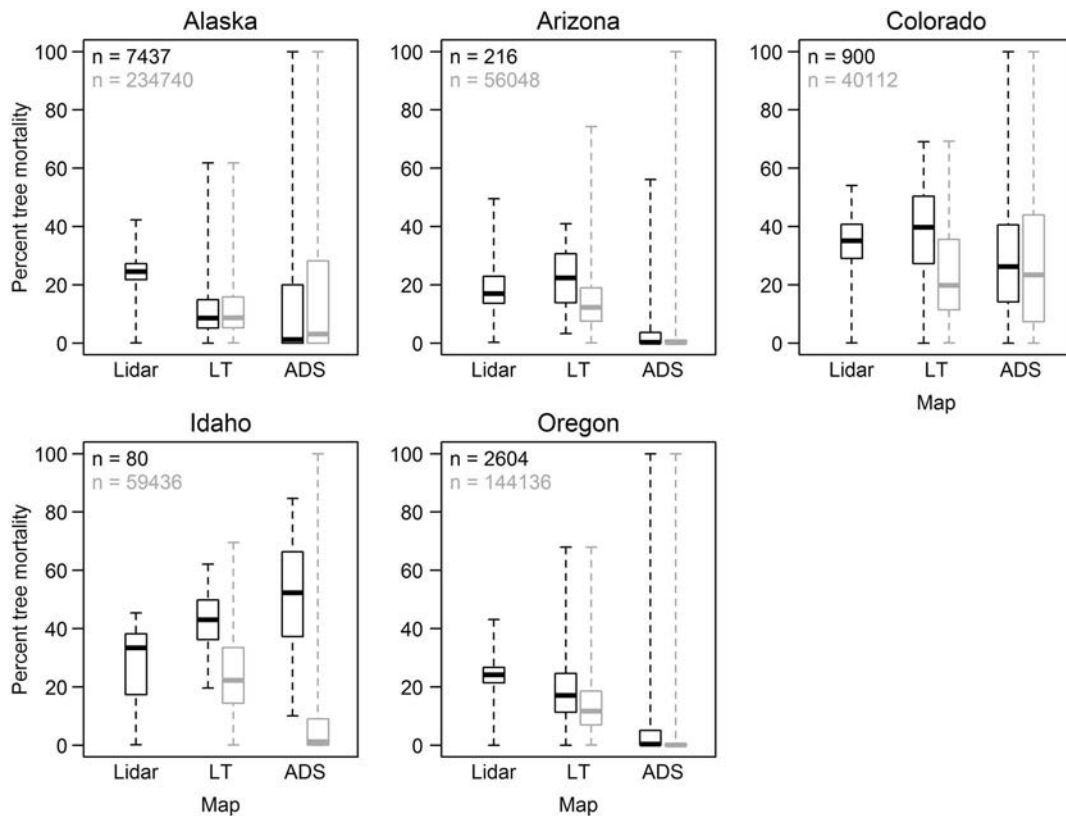
Fig. 6. Distributions of percent tree mortality in 1-km^2 grid cells from lidar-, LandTrendr (LT)-, and ADS-derived maps for each study area. Black boxplots correspond to distributions from forested lidar extents; gray boxplots correspond to distributions from forested LT extents. Grid cells disturbed by fire are not included in distributions. The numbers of grid cells in each distribution are given in the upper left corner of panels; black and gray text corresponds to lidar and LT extent distributions, respectively. Lidar and LT distributions are in terms of percent dead BA. ADS distributions are in terms of percent tree mortality area. Lidar and LT predictions were aggregated to 1-km spatial resolution for comparison with ADS data. Middle ADS estimates were used [1] and [62].

between LandTrendr and ADS estimates were greatest in these areas. In other words, high correlations in AK and CO may be indicative of a more simplified disturbance history across a large forested area. In OR, significant spruce budworm defoliation was also present and likely lowered correlations. Salvage logging of beetle-killed trees might have also caused disagreement between lidar, LandTrendr, and ADS estimates of mortality. Low correlations, as well as differences in distributions of % tree mortality between lidar, LandTrendr, and ADS data (Fig. 6), were also partly due to the fact that predictions were in different units; lidar and LandTrendr predictions were in units of %Dead BA, whereas ADS estimates were in units of % tree mortality area. Although %Dead BA and % tree mortality area are similar, they are not completely comparable.

Our analysis showed how lidar and LandTrendr could be used to predict BA conditions post-bark beetle outbreak. We did not investigate how well LandTrendr detected outbreak initiation or trajectories using yearly ADS data, or how well lidar and LandTrendr detected needle-on and needle-off stages of tree mortality. Beetle-killed trees retain dead needles, which are red and yellow in color, for a few years following death, after which needles begin to fall [28], [31]–[33]. Bark beetle-caused tree mortality generally occurred across our LandTrendr extents from 1987 to 2010. Most field and lidar data were collected near 2010, after outbreaks had been ongoing for several years, so most killed trees likely did not have needles at the time of

field and lidar data acquisition. The LandTrendr temporal extent ranged from 1984 to 2010, and thus captured canopy reflectance changes associated with beetle-caused tree mortality. Maps of %Dead BA showed that LandTrendr models were also sensitive to other types of forest disturbance, which necessitated the use of MTBS data to exclude areas burned by fire. Disturbance type differentiation by LandTrendr, which would have been useful to our analysis, is a topic for future research.

Our modeling results agree with those of previous studies. Like others, we found that lidar variables that measure forest vertical structure were better predictors of Total BA than variables from passive multispectral sensors [39], [40], [45]. Important predictors of Total and Live BA that we found, namely lidar density and height variables, were similar to what others have reported [39], [40], [44], [45], [55], [56]. Foliated branches will produce a more distributed canopy height profile than the greater lidar pulse penetration allowed through dead tree crowns, which equates to likely greater sensitivity of lidar metrics to healthy canopy conditions in these forest types, none of which are particularly dense. We found LandTrendr variables to be better predictors of Dead and %Dead BA; Pflugmacher *et al.* [45] found the same when predicting Dead BA caused by several types of disturbance. LandTrendr was likely a better predictor of Dead and %Dead BA because 1) lidar only represented a single snapshot of forest structure, whereas LandTrendr involved repeated measurements

capable of showing disturbance-caused change and 2) Landsat imagery used by LandTrendr captured spectral variability in forest canopies caused by bark beetle disturbance that lidar height measurements could not. Similar to us, Meigs *et al.* [44] and Pflugmacher *et al.* [45] found that Landsat disturbance magnitude variables were important predictors of Dead BA in disturbed forests. Our RF models that used LandTrendr variables explained variance of %Dead BA (48%) similarly to Meigs *et al.* [44] (40%). We predicted Live and Dead BA using LandTrendr variables less accurately (28%–51% variance explained) than Pflugmacher *et al.* [45] ($R^2 = 0.86$). However, unlike our plots where disturbance was caused by bark beetles only, most of the plots in Pflugmacher *et al.* [45] were disturbed by fire and harvest, which the LandTrendr algorithm likely detects more easily.

V. CONCLUSION

We predicted Total, Live, Dead, and %Dead BA in bark beetle-affected forests with moderate accuracy using RF models that used lidar and LandTrendr data as predictor variables. Lidar was a better predictor of Total and Live BA, whereas LandTrendr was a better predictor of Dead and %Dead BA. Predictions of %Dead BA generated from RF models were poorly to moderately correlated with estimates of tree mortality area generated from ADS data. Our results confirm the utility of LandTrendr for detecting and quantifying bark beetle-caused disturbance as has been demonstrated by others, but improve upon these studies by comparing predictions to ADS data, arguably the best available source of independent information for model evaluation. Such maps have immediate utility to managers and our modeling methodology, which generalized across five study areas with different forest types, could be replicated elsewhere in western North America by forest managers and researchers who need to quantify and map bark beetle-caused tree mortality.

REFERENCES

[1] A. J. H. Meddens, J. A. Hicke, and C. A. Ferguson, "Spatiotemporal patterns of observed bark beetle-caused tree mortality in British Columbia and the western United States," *Ecol. Appl.*, vol. 22, pp. 1876–1891, Oct. 2012.

[2] W. H. Romme, D. H. Knight, and J. B. Yavitt, "Mountain pine beetle outbreaks in the Rocky Mountains—Regulators of primary productivity," *Amer. Nat.*, vol. 127, pp. 484–494, Apr. 1986.

[3] M. Brown *et al.*, "Impact of mountain pine beetle on the net ecosystem production of lodgepole pine stands in British Columbia," *Agric. Forest Meteorol.*, vol. 150, pp. 254–264, Feb. 2010.

[4] N. C. Coops and M. A. Wulder, "Estimating the reduction in gross primary production due to mountain pine beetle infestation using satellite observations," *Int. J. Remote Sens.*, vol. 31, pp. 2129–2138, 2010.

[5] W. A. Kurz *et al.*, "Mountain pine beetle and forest carbon feedback to climate change," *Nature*, vol. 452, pp. 987–990, Apr. 2008.

[6] E. M. Pfeifer, J. A. Hicke, and A. J. H. Meddens, "Observations and modeling of aboveground tree carbon stocks and fluxes following a bark beetle outbreak in the western United States," *Global Change Biol.*, vol. 17, pp. 339–350, Jan. 2011.

[7] S. L. Edburg, J. A. Hicke, D. M. Lawrence, and P. E. Thornton, "Simulating coupled carbon and nitrogen dynamics following mountain pine beetle outbreaks in the western United States," *J. Geophys. Res. Biogeosci.*, vol. 116, pp. 1–15, Dec. 2011.

[8] J. A. Hicke *et al.*, "Effects of biotic disturbances on forest carbon cycling in the United States and Canada," *Global Change Biol.*, vol. 18, pp. 7–34, Jan. 2012.

[9] N. Bethlahmy, "More streamflow after a bark beetle epidemic," *J. Hydrol.*, vol. 23, pp. 185–189, 1974.

[10] E. Pugh and E. Small, "The impact of pine beetle infestation on snow accumulation and melt in the headwaters of the Colorado River," *Ecohydrology*, vol. 5, pp. 467–477, Jul. 2012.

[11] J. A. Biederman *et al.*, "Multiscale observations of snow accumulation and peak snowpack following widespread, insect-induced lodgepole pine mortality," *Ecohydrology*, vol. 7, pp. 150–162, Nov. 2012.

[12] T. L. O'Halloran *et al.*, "Radiative forcing of natural forest disturbances," *Global Change Biol.*, vol. 18, pp. 555–565, Feb. 2012.

[13] C. Wiedinmyer, M. Barlage, M. Tewari, and F. Chen, "Meteorological impacts of forest mortality due to insect infestation in Colorado," *Earth Interact.*, vol. 16, pp. 1–11, Feb. 2012.

[14] H. Maness, P. J. Kushner, and I. Fung, "Summertime climate response to mountain pine beetle disturbance in British Columbia," *Nat. Geosci.*, vol. 6, pp. 65–70, Nov. 2012.

[15] B. C. Bright, J. A. Hicke, and A. J. H. Meddens, "Effects of bark beetle-caused tree mortality on biogeochemical and biogeophysical MODIS products," *J. Geophys. Res. Biogeosci.*, vol. 118, pp. 974–982, Jul. 2013.

[16] A. C. A. Chan-McLeod, "A review and synthesis of the effects of unsalvaged mountain-pine-beetle-attacked stands on wildlife and implications for forest management," *BC J. Ecosyst. Manage.*, vol. 7, pp. 119–132, 2006.

[17] W. Klenner and A. Arsenault, "Ponderosa pine mortality during a severe bark beetle (Coleoptera: Curculionidae, Scolytinae) outbreak in southern British Columbia and implications for wildlife habitat management," *Forest Ecol. Manage.*, vol. 258, pp. S5–S14, Dec. 2009.

[18] M. J. Jenkins, E. Hebertson, W. Page, and C. A. Jorgensen, "Bark beetles, fuels, fires and implications for forest management in the Intermountain West," *Forest Ecol. Manage.*, vol. 254, pp. 16–34, Jan. 2008.

[19] J. A. Hicke, M. C. Johnson, L. H. D. Jane, and H. K. Preisler, "Effects of bark beetle-caused tree mortality on wildfire," *Forest Ecol. Manage.*, vol. 271, pp. 81–90, May 2012.

[20] R. E. Kennedy, Z. G. Yang, and W. B. Cohen, "Detecting trends in forest disturbance and recovery using yearly Landsat time series: 1. LandTrendr—Temporal segmentation algorithms," *Remote Sens. Environ.*, vol. 114, pp. 2897–2910, Dec. 2010.

[21] R. L. Furniss and V. M. Carolin, "Order Coleoptera—Beetles," in *Western Forest Insects*. Washington, DC, USA: USDA Forest Service, 1977, pp. 339–342.

[22] B. Bentz *et al.*, "Bark beetle outbreaks in western North America: Causes and consequences," in *Proc. Bark Beetle Symp.*, Snowbird, UT, USA, 2009, pp. 1–42.

[23] H. K. Preisler, J. A. Hicke, A. A. Ager, and J. L. Hayes, "Climate and weather influences on spatial temporal patterns of mountain pine beetle populations in Washington and Oregon," *Ecology*, vol. 93, pp. 2421–2434, Nov. 2012.

[24] B. J. Bentz *et al.*, "Climate change and bark beetles of the western United States and Canada: Direct and indirect effects," *Bioscience*, vol. 60, pp. 602–613, Sep. 2010.

[25] T. L. Shore and L. Safranyik, "Susceptibility and risk rating systems for the mountain pine beetle in lodgepole pine stands," Forestry Canada, Canadian Forestry Service, Pacific and Yukon Region, Vancouver, BC, Canada, Info. Rep. BC-X-336, 1992.

[26] K. F. Raffa *et al.*, "Cross-scale drivers of natural disturbances prone to anthropogenic amplification: The dynamics of bark beetle eruptions," *Bioscience*, vol. 58, pp. 501–517, Jun. 2008.

[27] A. J. H. Meddens, J. A. Hicke, L. A. Vierling, and A. T. Hudak, "Evaluating methods to detect bark beetle-caused tree mortality using single-date and multi-data Landsat imagery," *Remote Sens. Environ.*, vol. 132, pp. 49–58, May 2013.

[28] M. A. Wulder, C. C. Dymond, J. C. White, D. G. Leckie, and A. L. Carroll, "Surveying mountain pine beetle damage of forests: A review of remote sensing opportunities," *Forest Ecol. Manage.*, vol. 221, pp. 27–41, Jan. 2006.

[29] M. Gilichinsky, H. Olsson, and S. Solberg, "Reflectance changes due to pine sawfly attack detected using multitemporal SPOT satellite data," *Remote Sens. Lett.*, vol. 4, pp. 10–18, 2013.

[30] S. Solberg, E. Naesset, K. H. Hanssen, and E. Christiansen, "Mapping defoliation during a severe insect attack on Scots pine using airborne laser scanning," *Remote Sens. Environ.*, vol. 102, pp. 364–376, Jun. 2006.

[31] F. J. Ahern, "The effects of bark beetle stress on the foliar spectral reflectance of lodgepole pine," *Int. J. Remote Sens.*, vol. 9, pp. 1451–1468, Sep. 1988.

[32] J. M. Schmid, "Temperatures, growth, and fall of needles on Engelmann spruce infested by spruce beetles," USDA Forest Service, Rocky Mountain Forest and Range Experiment Station, Fort Collins, CO, USA, Research Note RM-331, 1976.

[33] A. J. H. Meddens, J. A. Hicke, and L. A. Vierling, "Evaluating the potential of multispectral imagery to map multiple stages of tree mortality," *Remote Sens. Environ.*, vol. 115, pp. 1632–1642, Jul. 2011.

[34] N. C. Coops *et al.*, "Assessing differences in tree and stand structure following beetle infestation using lidar data," *Can. J. Remote Sens.*, vol. 35, pp. 497–508, Dec. 2009.

[35] B. C. Bright, A. T. Hudak, R. McGaughey, H. E. Andersen, and J. Negron, "Predicting live and dead tree basal area of bark beetle affected forests from discrete-return lidar," *Can. J. Remote Sens.*, vol. 39, no. S1, pp. S99–S111, Sep. 2013.

[36] G. R. Hopping and G. Beall, "The relation of diameter of lodgepole pine to incidence of attack by the bark beetle Dendroctonus monticolae Hopkins," *For. Chron.*, vol. 24, pp. 141–145, 1948.

[37] R. Nelson, W. Krabill, and J. Tonelli, "Estimating forest biomass and volume using airborne laser data," *Remote Sens. Environ.*, vol. 24, pp. 247–267, Mar. 1988.

[38] M. A. Lefsky *et al.*, "Lidar remote sensing of above-ground biomass in three biomes," *Global Ecol. Biogeogr.*, vol. 11, pp. 393–399, Sep. 2002.

[39] A. T. Hudak *et al.*, "Regression modeling and mapping of coniferous forest basal area and tree density from discrete-return lidar and multispectral satellite data," *Can. J. Remote Sens.*, vol. 32, pp. 126–138, Apr. 2006.

[40] H. Latifi, A. Nothdurft, and B. Koch, "Non-parametric prediction and mapping of standing timber volume and biomass in a temperate forest: Application of multiple optical/LiDAR-derived predictors," *Forestry*, vol. 83, pp. 395–407, Oct. 2010.

[41] W. B. Cohen and S. N. Goward, "Landsat's role in ecological applications of remote sensing," *Bioscience*, vol. 54, pp. 535–545, Jun. 2004.

[42] C. Huang *et al.*, "An automated approach for reconstructing recent forest disturbance history using dense Landsat time series stacks," *Remote Sens. Environ.*, vol. 114, pp. 183–198, 2010.

[43] J. G. Masek *et al.*, "United States forest disturbance trends observed using Landsat time series," *Ecosystems*, vol. 16, no. 6, pp. 1087–1104, 2013.

[44] G. W. Meigs, R. E. Kennedy, and W. B. Cohen, "A Landsat time series approach to characterize bark beetle and defoliator impacts on tree mortality and surface fuels in conifer forests," *Remote Sens. Environ.*, vol. 115, pp. 3707–3718, Dec. 2011.

[45] D. Pflugmacher, W. B. Cohen, and R. E. Kennedy, "Using Landsat-derived disturbance history (1972–2010) to predict current forest structure," *Remote Sens. Environ.*, vol. 122, pp. 146–165, Jul. 2012.

[46] M. Main-Knorn *et al.*, "Monitoring coniferous forest biomass change using a Landsat trajectory-based approach," *Remote Sens. Environ.*, vol. 139, pp. 277–290, Dec. 2013.

[47] J. Wallerman and J. Holmgren, "Estimating field-plot data of forest stands using airborne laser scanning and SPOT HRG data," *Remote Sens. Environ.*, vol. 110, pp. 501–508, Oct. 2007.

[48] M. Maltamo, J. Malinen, P. Packaln, A. Suvanto, and J. Kangas, "Non-parametric estimation of stem volume using airborne laser scanning, aerial photography, and stand-register data," *Can. J. Forest Res.*, vol. 36, pp. 426–436, Feb. 2006.

[49] S. Tonolli *et al.*, "Fusion of airborne LiDAR and satellite multispectral data for the estimation of timber volume in the Southern Alps," *Remote Sens. Environ.*, vol. 115, pp. 2486–2498, 2011.

[50] J. L. Strunk, H. Temesgen, H. E. Andersen, and P. Packalen, "Prediction of forest attributes with field plots, Landsat, and a sample of lidar strips: A case study on the Kenai Peninsula, Alaska," *Photogramm. Eng. Remote Sens.*, vol. 80, pp. 143–150, Feb. 2014.

[51] M. Mutlu, S. C. Popescu, C. Stripling, and T. Spencer, "Mapping surface fuel models using lidar and multispectral data fusion for fire behavior," *Remote Sens. Environ.*, vol. 112, pp. 274–285, Jan. 2008.

[52] T. L. Erdody and L. M. Moskal, "Fusion of LiDAR and imagery for estimating forest canopy fuels," *Remote Sens. Environ.*, vol. 114, pp. 725–737, Apr. 2010.

[53] USDA Forest Service, "Major forest insect and disease conditions in the United States: 2009 update," Forest Health Protection, Washington, DC, USA, Rep. FS-952, 2010.

[54] L. Breiman, "Random forests," *Mach. Learn.*, vol. 45, pp. 5–32, Oct. 2001.

[55] A. T. Hudak, N. L. Crookston, J. S. Evans, D. E. Hall, and M. J. Falkowski, "Nearest neighbor imputation of species-level, plot-scale forest structure attributes from LiDAR data," *Remote Sens. Environ.*, vol. 112, pp. 2232–2245, 2008.

[56] A. T. Hudak *et al.*, "Quantifying aboveground forest carbon pools and fluxes from repeat LiDAR surveys," *Remote Sens. Environ.*, vol. 123, pp. 25–40, 2012.

[57] N. L. Crookston and G. E. Dixon, "The forest vegetation simulator: A review of its structure, content, and applications," *Comput. Electron. Agric.*, vol. 49, no. 1, pp. 60–80, 2005.

[58] G. E. Dixon, *Essential FVS: A User's Guide to the Forest Vegetation Simulator*. Fort Collins, CO, USA: USDA Forest Service, Forest Management Service Center, 2008.

[59] R. J. McGaughey, *FUSION/LDV: Software for LiDAR Data Analysis Visualization*. Portland, OR, USA: USDA Forest Service, Pacific Northwest Research Station, Feb. 2013.

[60] J. W. van Wagtendonk, R. R. Root, and C. H. Key, "Comparison of AVIRIS and Landsat ETM+ detection capabilities for burn severity," *Remote Sens. Environ.*, vol. 92, pp. 397–408, Aug. 2004.

[61] E. P. Crist, "A TM tasseled cap equivalent transformation for reflectance factor data," *Remote Sens. Environ.*, vol. 17, pp. 301–306, 1985.

[62] J. A. Hicke, A. J. H. Meddens, C. D. Allen, and C. A. Kolden, "Carbon stocks of trees killed by bark beetles and wildfire in the western United States," *Environ. Res. Lett.*, vol. 8, pp. 1–8, Aug. 2013.

[63] R Core Team, *R: A Language and Environment for Statistical Computing*. Vienna, Austria: R Foundation for Statistical Computing, 2013 [Online]. Available: http://www.R-project.org/

[64] A. Liaw and M. Wiener, "Classification and regression by randomForest," *R News*, vol. 2, no. 3, pp. 18–22, 2002.

[65] M. A. Murphy, J. S. Evans, and A. Storfer, "Quantifying Bufo boreas connectivity in Yellowstone National Park with landscape genetics," *Ecology*, vol. 91, pp. 252–261, 2010.

[66] J. S. Evans and S. A. Cushman, "Gradient modeling of conifer species using random forests," *Landscape Ecol.*, vol. 24, pp. 673–683, May 2009.

[67] J. S. Evans, M. A. Murphy, Z. A. Holden, and S. A. Cushman, "Modeling species distribution and change using Random Forests" in *Predictive Modeling in Landscape Ecology*. New York, NY, USA: Springer, 2011, ch. 8, pp. 139–159.

[68] B. Ruefenacht *et al.*, "Conterminous US and Alaska forest type mapping using forest inventory and analysis data," *Photogramm. Eng. Remote Sens.*, vol. 74, pp. 1379–1388, Nov. 2008.

[69] J. Eidenshink *et al.*, "A project for monitoring trends in burn severity," *Fire Ecol.*, vol. 3, no. 1, pp. 3–21, 2007.

[70] E. P. Crist and R. C. Cicone, "A physically-based transformation of thematic mapper data—The TM Tasseled Cap," *IEEE Trans. Geosci. Remote Sens.*, vol. 22, no. 3, pp. 256–263, May 1984.

[71] R. S. Skakun, M. A. Wulder, and S. E. Franklin, "Sensitivity of the thematic mapper enhanced wetness difference index to detect mountain pine beetle red-attack damage," *Remote Sens. Environ.*, vol. 86, pp. 433–443, Aug. 2003.

[72] J. M. Schmid and R. H. Frye, "Stand ratings for spruce beetles," USDA Forest Service, Rocky Mountain Research Station, Fort Collins, CO, USA, Res. Paper RM-309, 1976.

[73] G. G. Parker and M. E. Russ, "The canopy surface and stand development: Assessing forest canopy structure and complexity with near-surface altimetry," *Forest Ecol. Manage.*, vol. 189, pp. 307–315, Feb. 2004.

Benjamin C. Bright received the B.S. degree in geography from Brigham Young University, Provo, UT, USA, in 2009, and the M.S. degree in environmental science from the University of Idaho, Moscow, ID, USA, in 2011.

From 2011 to 2013, he was a Research Associate with the University of Idaho. In 2013, he became a Geographer with the U.S. Forest Service Rocky Mountain Research Station, Moscow, ID, USA. His research interests include remote sensing of vegetation, and forest, woodland, and rangeland disturbance and ecology.

Andrew T. Hudak received the B.S. degree in ecology, evolution, and behavior from the University of Minnesota, St. Paul, MN, USA, in 1990, and the Ph.D. degree in environmental, population, and organismic biology from the University of Colorado, Boulder, CO, USA, in 1999.

From 1990 to 1992, he served with the U.S. Peace Corps, Malawi, Southeast Africa. In 1999, he became a Research Ecologist with the U.S. Forest Service Pacific Northwest Research Station, Corvallis, OR, USA, and in 2001, began his current position as a Research Forester with the Rocky Mountain Research Station in Moscow, ID, USA. His research interests include landscape, vegetation, and fire ecology; remote sensing of vegetation patterns and processes; forest and rangeland ecology and management; and predictive modeling of spatially explicit ecological data.

Robert E. Kennedy received the B.S. degree in biology from the University of Houston, Houston, TX, USA, in 1992, the M.A. degree in biology from the University of Colorado, Boulder, CO, USA, in 1994, and the Ph.D. degree in forest science from Oregon State University, Corvallis, OR, USA, in 2004.

He was a Faculty Research Assistant during his time as a graduate student at Oregon State University. From 2004 to 2008, he was a Postdoctoral Research Ecologist with the U.S. Forest Service Pacific Northwest Research Station, Corvallis, OR, USA. In 2008, he became a Research Associate with the Department of Forest Ecosystems, Oregon State University, and became an Assistant Professor and Senior Researcher for the same department in 2010. In 2012, he joined as an Assistant Professor with the Department of Earth and Environment, Boston University, Boston, MA, USA. His research interests include the unique perspective afforded by remote sensing to better understand the processes and drivers that cause changes in ecosystems and landscapes.

Arjan J. H. Meddens received the B.S. degree in forest and nature conservation and the M.S. degree in geo-information systems and remote sensing from Wageningen University, Wageningen, The Netherlands, in 2004 and 2007, respectively, and the Ph.D. degree in environmental science from the University of Idaho, Moscow, ID, USA, in 2012.

From 2002 to 2003, he worked as a Student and Research Assistant and became a Graduate Researcher with Wageningen University in 2004. From 2004 to 2005, he performed his thesis research at Landcare Research, New Zealand. In 2006, he came to the United States as a Research Intern with the U.S. Forest Service Rocky Mountain Station, Moscow, ID, USA. From 2007 to 2012, he worked as a Research Assistant with the University of Idaho while pursuing his doctorate degree. Since 2012, he has been a Postdoctoral Fellow with the Department of Geography, University of Idaho, Moscow, ID, USA. His research interests include forest ecology, remote sensing, carbon cycling, and forest disturbance.